Engineering Structures 200 (2019) 109692

Contents lists available at ScienceDirect

Engineering Structures

journal homepage: www.elsevier.com/locate/engstruct

Adhesively bonded glass-metal façade elements with composite structural behaviour under in-plane and out-of-plane loading

Vlad Alexandru Silvestru[a,1,*], Georg Kolany[a,2], Bernhard Freytag[b], Jens Schneider[c], Oliver Englhardt[a,3]

[a] Institute of Building Construction, Graz University of Technology, Lessingstraße 25, 8010 Graz, Austria
[b] Laboratory for Structural Engineering, Graz University of Technology, Inffeldgasse 24, 8010 Graz, Austria
[c] Institute of Structural Mechanics and Design, Technische Universität Darmstadt, Franziska-Braun-Straße 3, 64287 Darmstadt, Germany

ARTICLE INFO

Keywords:
Composite structural behaviour
Glass-metal shear panel
Linear adhesive bonding
Grouting
Multiaxial large-scale testing
Non-linear simulation

ABSTRACT

The structural efficiency of transparent façades can be increased by achieving a composite structural behaviour between the framing elements and the glass panes. The use of suitable intermediary materials is substantial for obtaining a composite structural behaviour for both out-of-plane and in-plane loading. This article presents two novel configurations for such glass-metal elements. For the first configuration, a perimetrical bonding with a silicone adhesive between the glass pane and the filigree metal framing is responsible for transferring stresses in out-of-plane direction, and grouting blocks are used near the glass pane corners for transferring stresses in in-plane direction. In the case of the second configuration, a perimetrical bonding with an acrylic adhesive between the glass pane and the filigree metal framing is responsible for transferring stresses in both out-of-plane and in-plane direction. Full-scale tests and finite element simulations with loads acting in three different directions, both separately and combined, are performed for the two configurations. The results of the tests performed under in-plane shear loading reveal a high load-bearing capacity of both configurations and show that failure is initiated within the adhesive joints. The numerical models, which include previously derived non-linear material models for the adhesives, allow a good prediction of the mechanical response of the investigated glass-metal elements. The presented load vs. displacement diagrams illustrate that the elements with acrylic adhesive behave stiffer both under out-of-plane and under in-plane loading before the adhesive starts to yield. Overall, the configuration with silicone adhesive and grouting represents a solution which can be applied in real projects based on existing technical approvals for the involved materials in similar applications. On the other hand, the configuration with acrylic adhesive indicates the potential of glass-metal elements with stiffer adhesives, assuming that the knowledge on such adhesives will continue to grow and that, eventually, new enhanced products will be developed by the adhesive industry.

1. Introduction

Highly transparent facades are one of the distinctive aspects of many iconic office buildings completed during the last decades. Whether post-and-beam facades, also known as stick-systems, unitised facades or double-skin facades, often, the load-bearing structure of such building envelopes consists of linear elements made of opaque materials like aluminium or stainless steel, while the glass panes act only as infill elements. The demands for efficiency of the buildings and implicitly of their facades are constantly increasing from different points of view (e.g. energy efficiency, efficient material use, structural efficiency). Regarding a highly efficient use of materials, a possibility to design elegant transparent building envelopes is to activate a composite structural behaviour between the glass panes and the metal framing. While a significant amount of knowledge is available from previous research for the structural behaviour of the different materials separately, this article contributes with novel findings regarding the interaction of the materials in a glass-metal façade element and the structural performance of such elements.

An analysis of the utilisation types of the material glass in the construction field reveals that the highest percentage of glass panes is

* Corresponding author at: Tulpenstrasse 43, 8051 Zürich, Switzerland.
E-mail addresses: silvestru_vlad@yahoo.com (V.A. Silvestru), georg.kolany@daninger.at (G. Kolany), freytag@tugraz.at (B. Freytag), schneider@ismd.tu-darmstadt.de (J. Schneider), office@englhardt-engineering.com (O. Englhardt).
[1] Now employed at Dr. Lüchinger + Meyer Bauingenieure AG, Zürich, Switzerland.
[2] Now employed at Daninger & Partner Ziviltechniker KG, Graz, Austria.
[3] Now managing partner at Englhardt Engineering, Munich, Germany.

https://doi.org/10.1016/j.engstruct.2019.109692
Received 4 April 2019; Received in revised form 11 August 2019; Accepted 16 September 2019
0141-0296/ © 2019 Elsevier Ltd. All rights reserved.

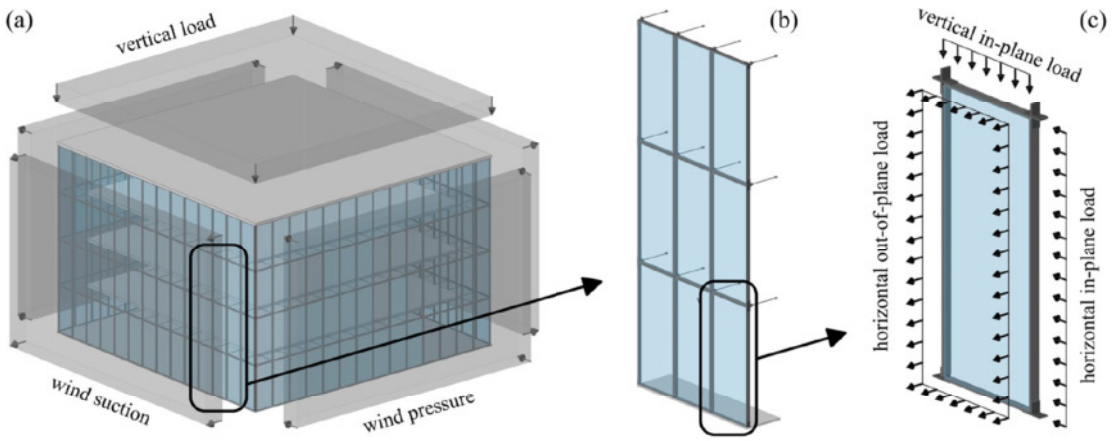

Fig. 1. Principle of adhesively bonded glass-metal façade elements with composite structural behaviour illustrated for the outer layer of a double skin façade at building level (a), at façade level (b) and at element level (c).

used in glazed building envelopes and the structural function of these glass panes is limited to bearing out-of-plane loads. However, considering the structural capacity of glass, more efficient systems are possible for transparent facades in certain situations by aiming an optimised use of the installed materials (see also ideas discussed by Englhardt in [1]). Single-storey pavilions with in-plane loaded glass walls are examples of realised projects with such systems. The glass-metal elements investigated in this article can also be used for such pavilions, but are rather thought to be suitable systems for self-supporting transparent façades extending over more than one storey. The elements have a sufficient in-plane rigidity and only need additional out-of-plane supports depending on their size. An example for an application of such a self-supporting façade is the outer layer of a double-skin façade as the one illustrated schematically in Fig. 1a. The elements forming this kind of façade consist of a glass pane, which acts as a shear panel and ensures the necessary in-plane rigidity, and a filigree metal framing, which provides a certain out-of-plane support for the glass pane and allows for mechanical connections between several elements as well as between elements and other structural components. The necessary out-of-plane support of the elements can be realized point-wise with hinged rods in their corners (see Fig. 1b). Such a façade can be generally subjected to vertical loads as for example the dead weight of the elements and by horizontal loads as for example wind loads. This results in vertical and horizontal in-plane loads as well as in horizontal out-of-plane loads on the elements (see Fig. 1c). The main difference between the introduced façade system, consisting of glass-metal elements with composite structural behaviour, and mainstream curtain wall constructions, is the systematic bearing of loads in in-plane direction by the façade without additional bracing elements.

In this article, two systems for glass-metal elements with composite structural behaviour are investigated. Before introducing the two novel configurations, which differ in terms of the stress transfer between the glass pane and the metal framing, and before presenting the results obtained for these two configurations, a brief background on previous experimental investigations on in-plane and out-of-plane loaded glass panes is provided.

2. Background on in-plane and out-of-plane loaded glass panes

This background focuses on in-plane and out-of-plane loaded glass panes with the dimensions in two directions significantly larger than their thickness. Therefore, glass beams like those presented in the comprehensive review on composite glass beams by Martens et al. [2] are not included. Furthermore, mainly studies on glass panes connected to a metal framing are covered. Research performed on glass-timber elements is not included in this summary.

In terms of in-plane loaded glass panes a differentiation in *(i)* glass panes loaded by uniaxial compression (see Fig. 2a), *(ii)* glass panes activated as a bracing (see Fig. 2b) and *(iii)* glass panes activated as a shear panel (see Fig. 2c) can be made. All previously investigated systems had either a metal framing with a high out-of-plane stiffness along the perimeter of the glass panes, which acted as a rigid support for the glass pane edges, or only local out-of-plane supports near the glass pane corners. The previous studies focused mainly on the plate buckling of

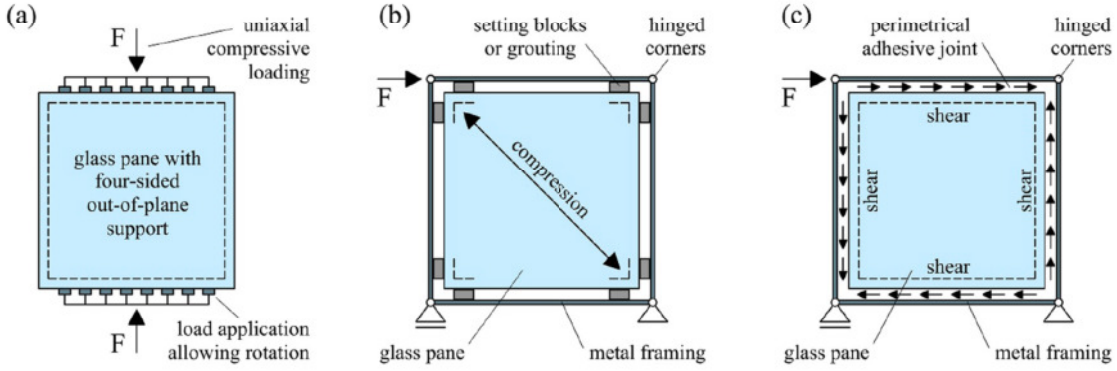

Fig. 2. Different previously investigated systems for in-plane loaded glass panes: glass panes loaded by uniaxial compression (a), glass panes loaded by in-plane shear as a bracing (b) and glass panes loaded by in-plane shear as a shear panel (c).

Table 1
Characteristics of previous experimental investigations on in-plane loaded glass panes with metal support structures.

Literature reference	Loading type	Glass pane dimensions [m]	Glass pane thickness[a] [mm]	Stress transfer between framing and glass pane	Steel framing top & bottom	Lateral	Out-of-plane support of the glass pane
Luible [3]	Uniaxial compression	1.0 × 1.0 m	MG 6 to 10 mm	Along two opposite edges with soft aluminium layers	UNP 180	IPE 160	Four-sided along the perimeter (rotation allowed)
Englhardt [4]	Uniaxial compression	1.0 × 1.0 m up to 2.0 × 1.0 m	MG 4 to 8 mm LG 2 × 4 mm	Along two opposite edges and local near the glass pane corners with layers made of polyoxymethylene (POM)	HEB 300	UNP 200	Four-sided along the perimeter (rotation allowed)
Haese [5]	Uniaxial compression	1.0 × 1.5 m and 1.5 × 1.0 m	MG 8 mm	Local near the glass pane corners with setting blocks made of POM	None	Folded U-profile	Two-sided along the lateral edges and local at the load application points
Wellershoff [6]	In-plane shear (bracing)	1.2 × 1.2 m and 1.6 × 1.6 m	MG 4 to 10 mm LG 2 × 4 & 2 × 10 mm	Local with grouting in the diagonally cut corners of the glass pane	HEB 200	HEB 200	Local in the corners of the glass pane
Freitag & Wörner [7]	In-plane shear (bracing)	1.0 × 1.0 m	MG 8 mm LG 2 × 4 mm	Prestressed setting blocks made of POM near the glass pane corners or perimetrical prestressed elastomer	Not specified	Not specified	Local in the area of the setting blocks or perimetrical in the area of the elastomer
Wellershoff [6]	In-plane shear (shear panel)	1.2 × 1.2 m and 1.6 × 1.6 m	MG 4 & 6 mm LG 2 × 4 mm IG different setups	Linear adhesive bonding along the perimeter with acrylic and polyurethane adhesives	HEB 200	HEB 200	Four-sided along the perimeter
Huveners [8]	In-plane shear (shear panel)	1.0 × 1.0 m	MG 12 mm	Linear adhesive bonding along the perimeter with polyurethane and epoxy adhesives	120 × 60 mm (solid profile)	120 × 60 mm (solid profile)	Four-sided along the perimeter
Van Lancker et al. [9]	In-plane shear (shear panel)	1.5 × 3.5 m	MG 2 × 10 mm	Linear adhesive bonding along the perimeter with silicone adhesive	100 × 50 × 3 mm	100 × 50 × 3 mm	Local lateral torsional buckling restraints
Mocibob [11]	Combined uniaxial compression, in-plane shear and out-of-plane loading	1.2 × 3.5 m	LG 2 × 8 mm	Combined linear silicone adhesive and local grouting blocks at the top and bottom edges	HEB 180	HEB 180	Two-sided along the top and the bottom edges

[a] MG – monolithic glass, LG – laminated glass, IG – insulating glass.

the glass pane and on different materials for connecting the glass pane to the metal framing. An overview of the characteristics of previously experimentally investigated glass panes under in-plane loading at selected boundary conditions is provided in Table 1.

Glass panes with all edges supported out-of-plane and loaded uniaxially in-plane on two opposite edges are susceptible to plate buckling due to their slenderness. Such glass panes were investigated by Luible [3] and by Englhardt [4]. Both show that the glass panes subjected to plate buckling can carry loads which are higher than the critical buckling load, due to a post-critical load-bearing behaviour by activation of membrane forces. Moreover, they evaluate the effects of geometric and material parameters on the plate buckling behaviour of glass panes. According to their conclusions, non-linear finite element simulations are generally considered more suitable for buckling calculations than analytic approaches based on buckling curves. Another research on glass panes under uniaxial compression was carried out by Haese [5], focusing on the structural behaviour of glass panes with additional edge beams along the two unloaded edges and different load application concepts on such systems. His results show that applying the load on the edge beams alone allows a higher load-bearing capacity of the system compared to applying the load on both the glass pane and the edge beams.

An increase of the in-plane stiffness of a rectangular framing with no or low corner stiffness can be achieved either by diagonal struts or by activation of an infill element as a shear panel. These two possibilities are followed as well when the activation of glass panes as in-plane load bearing elements is aimed. To activate the glass pane as a diagonal strut, setting blocks or grouting are used near the glass pane corners as in the systems investigated by Wellershoff [6] (glass panes with grouting at the glass edge in the diagonally cut corners) or by Freitag & Wörner [7] (mechanically prestressed glass panes in order to introduce a compressive prestress state into the tension diagonal). Generally, the materials used for the setting blocks and the grouting allow a separation in case of tensile loads and therefore only activate the diagonal under compression. For such systems large deformations due to buckling along the compressed diagonal are observed before failure.

To obtain a shear panel, a perimetrical structural connection of the glass pane to the framing is required. This can be achieved with linear adhesive connections with sufficient shear stiffness, as in the systems investigated by Wellershoff [6] (two-sided adhesive bonding along the perimeter of the glass pane) or by Huveners [8] (one-sided, two-sided and edge-sided adhesive bonding along the perimeter of the glass pane). Both conclude that a high shear stiffness of the adhesives is necessary for such systems. Furthermore, both focus on deriving analytical approaches for the design of such systems.

Van Lancker et al. [9] investigated as well a system with glass panes activated as shear panels by linear adhesive bonding. The used configuration consisted of a frame made of cold-formed steel tubular profiles with adhesively bonded glass panes on both sides and was inspired from similar constructions with opaque structural sheeting screwed onto frames to provide them a resistance to in-plane loads. The results of the experiments showed, that this kind of hybrid glass-steel system can reach similar racking strengths as the more common systems with sheeting made of oriented strand boards. With respect to this type of system, Van Lancker et al. [10] address the mechanical behaviour of linear glass-steel connections with silicone adhesives under cyclic loading.

A system which combines the concepts of diagonal struts and shear panels was investigated by Mocibob [11] for one-storey-high glass pavilions. The glass panes were supported out-of-plane only along the top and bottom edges. An activation of both the compressive and the tensile diagonal was obtained: *(i)* the compressive one by grouting blocks and *(ii)* the tensile one by the linear adhesive bonding. Large deformations and a rather small resistance were observed for such panels under in-plane shear loading. For this system a study by finite element simulations on the effect of additional adhesively bonded vertical steel mullions on the buckling behaviour of the elements under in-plane shear loading was carried out by Amadio & Bedon [12].

In terms of out-of-plane loaded glass panes, Nhamoinesu [13] and Pascual et al. [14] investigated medium-scale (700 mm × 300 mm) and large-scale (3500 mm × 1500 mm) steel-glass composite units subjected to flexural loads. The units consisted of two glass sheets with tubular steel profile reinforcements between them, either only along their longitudinal edges or both along their longitudinal and transversal edges. The glass sheets and the steel profiles were bonded adhesively with a high strength adhesive. The results showed that the investigated steel-glass units exhibit substantial composite action as well as a certain post-fracture strength. Moreover, shear lag effects were noticed, especially in the case of the large-scale units. Pascual et al. [15] presents an analytical model for predicting deflections and strains of adhesively bonded GFRP-glass sandwich beams subjected to bending about the minor axis. This analytical model, which is able to take shear lag effects into consideration, is also applicable for the steel-glass units investigated by Nhamoinesu [13] and by Pascual et al. [14], due to their similar assembly compared to the sandwich beams.

Bedon et al. [16] presents preliminary results from finite element simulations on a novel prototype of a GFRP-glass sandwich unit to be used in facades. The prototype was developed based on the findings from Nhamoinesu [13], Pascual et al. [14] and Pascual et al. [15] and shows a slightly better performance from structural (bending about the minor axis) and thermal points of view compared to traditional façade systems with non-integrated aluminium profiles.

Hoffmeister et al. [17] investigated three different prototypes consisting of cold-bent glass panes, which are adhesively bonded to metal frames. The tests of the prototypes under out-of-plane loading in both directions, simulating wind pressure and wind suction, showed, beside the structural capacity of such systems, that in case of pressure the failure occurs always in the glass, while in case of suction failure in the adhesive is observed as well.

A large amount of the findings from the summarised research on in-plane and out-of-plane loaded glass panes are considered for the investigations presented in this article. However, the introduced novel configurations differ from most of the previous investigated systems, especially those under in-plane loading, in general by the fact, that the metal framing bonded to the glass pane along its perimeter is rather filigree. Therefore, this framing only provides a limited out-of-plane support to the glass pane edges. Other noteworthy characteristics, which define the distinctiveness of the performed investigations, are given by the stress transfer concepts between glass pane and metal framing and by the applied multiaxial loading on the specimens. The main objectives of the presented investigations are *(i)* to determine the structural behaviour of the introduced glass-metal elements with composite structural behaviour under different loading scenarios, *(ii)* to evaluate the possible failure modes of such elements and *(iii)* to validate finite element models which can be used in further simulations to assess the effect of various parameters on the structural behaviour of such elements.

3. Materials and methods

3.1. Design and assembly of the test specimens

The test specimens for glass-metal elements with composite structural behaviour consist of a glass pane and a filigree metal framing. The framing itself is composed of edge elements which provide a certain out-of-plane stiffness and corner elements which define the rigidity between the edge elements (see Fig. 3). For the connection between the glass pane and the metal framing, perimetrical adhesive bonding is considered to be the appropriate joining method, since it enables a more uniform load transfer. Based on the type of loads which have to be transferred and on the properties of the adhesives available on the market, two different configurations are followed in the design of the test specimens for glass-metal elements with composite structural behaviour: *(i)* Type 1 has a perimetrical bonding with a silicone adhesive

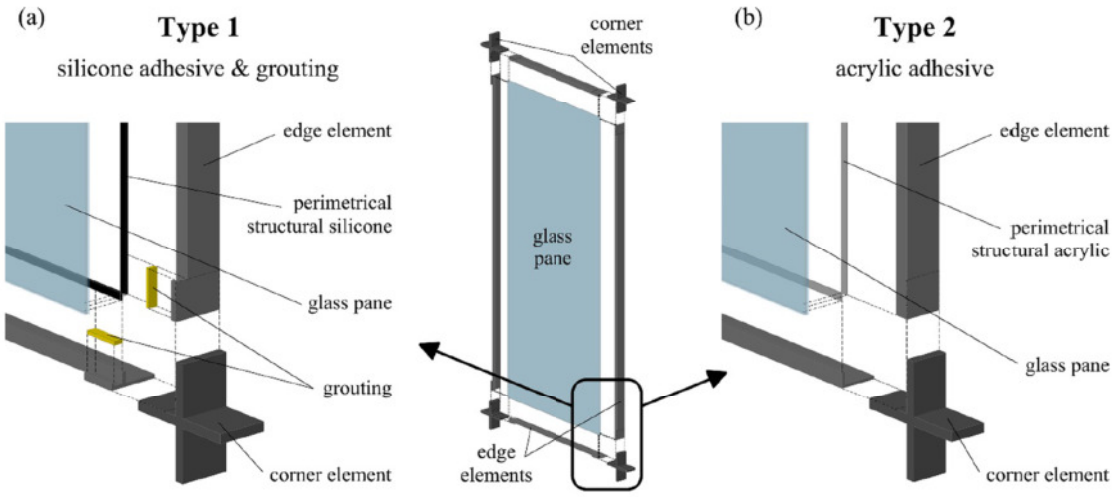

Fig. 3. Components of the two investigated systems for adhesively bonded glass-metal façade elements with composite structural behaviour: (a) system with silicone adhesive bonding along the perimeter of the glass pane and grouting in the corners and (b) system with acrylic adhesive bonding along the perimeter of the glass pane.

between the glass pane and the metal framing to transfer stresses in out-of-plane direction and additional grouting blocks near the glass pane corners to transfer stresses in in-plane direction (see Fig. 3a); *(ii)* Type 2 has a perimetrical bonding between the glass pane and the framing with an acrylic adhesive, which has to transfer both stresses in out-of-plane and in-plane direction (see Fig. 3b).

The size of the glass pane with a height of 3.5 m and a width of 1.5 m is chosen based on common dimensions for a storey-high glazing in office buildings. A total of four specimens are evaluated in this article, two of Type 1 and two of Type 2. For each of the two systems, one specimen has a monolithic 10 mm thick thermally toughened glass (TTG) pane (Type 1A and Type 2A), whereas the glass pane for the second specimen is a laminated glass made of two 6 mm thick thermally toughened glass sheets with a 1.52 mm thick polyvinyl butyral (PVB) interlayer (Type 1B and Type 2B). Although the performed investigations are limited at monolithic and laminated glass panes, the two systems are designed in such a way, that the configurations can be applied for insulating glazing as well, by adding the desired cavities and glass packages to the exterior, while only the interior glass package is activated from a structural point of view.

The geometry of the metal framing with all the main dimensions for the edge elements and for the corner elements are provided in Fig. 4 for the specimens of Type 1 and in Fig. 5 for the specimens of Type 2. These dimensions are results of simplified calculations aiming a reduced risk of undesired failure within the metal framing during testing and are therefore rather conservative.

The corner elements are made of structural steel 1.0045 (S355JR), whereas the edge elements are made of stainless steel 1.4404. The surfaces of the stainless steel on which the adhesives are applied are grinded with an abrasive paper P300. The geometry of the corner elements is designed in order to allow the fixing to the abutment block at one end of the glass-metal elements and the application of the in-plane loads at the other end. Welded connections are used between the corner elements and the edge elements in order to exclude the influence of an eventual slip which could occur in the case of bolted connections.

Table 2 summarizes the main characteristics and significant dimensions of the different components of the four test specimens.

3.1.1. *Characteristics of the applied structural adhesives*

The adhesives used for the two different systems of Type 1 and of Type 2 are chosen based on results from previous research on adhesives for linear structural glass-metal connections. Among others, the results presented by Belis et al. [20], by Overend et al. [21] and by Abeln et al. [22] as well as the previously mentioned research conducted by Wellershoff [6], Huveners [8] and Mocibob [11] are used as a basis. Furthermore, it is aimed on the one hand to use adhesives which are already approved by authorities for structural connections with glass substrates in the façade industry. On the other hand, however, adhesives with high shear stiffness and strength are searched in order to be able to transfer stresses between the glass pane and the metal framing in both in-plane and out-of-plane direction. These two considerations result in the two selected structural adhesives.

For the system of Type 1, the structural silicone Dow Corning® 993 [18] (currently Dowsil™ 993) is chosen, which is probably the adhesive for structural glass applications with the most available research results. For example, Hagl [23] presents results from tensile, shear and compressive tests and analyses the suitability of the hyperelastic material law by Mooney-Rivlin and Dias et al. [24] investigate a novel developed constitutive hyperelastic material law. Moreover Staudt et al. [25] analyse the applicability of available failure criteria for rubber-like materials, Rosendahl et al. [26] investigate failure properties of thick-layered structural silicone sealants and Rosendahl et al. [27] propose an equivalent strain failure criterion for multiaxially loaded incompressible hyperelastic elastomers, all based on Dow Corning® 993. This silicone adhesive also has a technical approval for the application in structural sealant glazing systems and has the advantage that its properties do not significantly degrade over time under the influence of moisture, UV-radiation and temperatures between −20 °C and +80 °C. Furthermore, results from investigations at material level and at connection level with Dow Corning® 993 related to the configuration used for the system of Type 1 as well as parameters determined for the hyperelastic material model by Mooney-Rivlin can be found in Silvestru [28] and in Silvestru et al. [29]. Due to its rather low shear stiffness, this adhesive is considered only for transferring stresses in out-of-plane direction, while for the stresses in in-plane direction additional local grouting near the glass pane corners is applied.

For the system of Type 2, the structural acrylic SikaFast®-5221 NT [19] is chosen based on results obtained for a similar product by Wellershoff [6] (double-lap shear tests and connection to a steel frame along the perimeter of square glass panes), Belis et al. [20] (single-lap shear tests both before and after artificial aging) and Abeln et al. [22] (application in hybrid steel-glass beams). Due to its higher shear stiffness and strength, this adhesive is considered to be able to transfer both the occurring stresses in out-of-plane and in-plane direction between

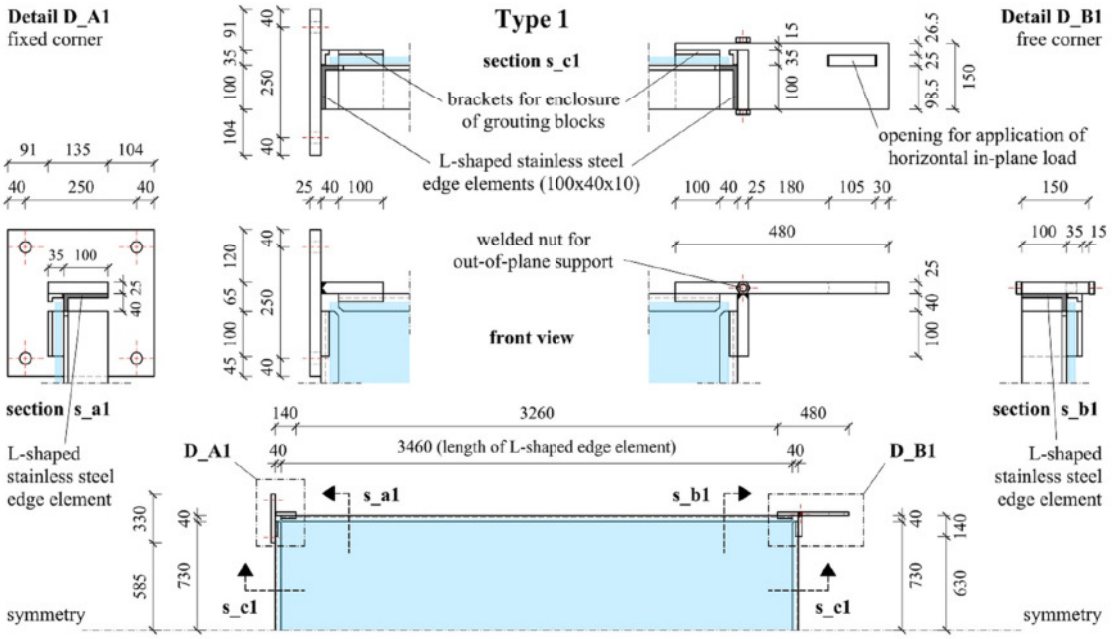

Fig. 4. Dimensions of the metal framing for the large-scale test specimen of Type 1 in [mm].

the glass pane and the metal framing without using additional grouting. Results from investigations at material level and at connection level with SikaFast®-5221 NT related to the configuration used for the system of Type 2 as well as parameters determined for a strain rate dependent plastic material model can be found in Silvestru [28] and in Silvestru et al. [30].

3.1.2. Characteristics of the applied injection grout

For the system of Type 1 the silicone adhesive along the perimeter of the glass pane is considered not stiff enough to obtain the desired composite structural behaviour between the glass pane and the metal framing. Therefore, a total of eight local blocks are positioned near the corners of the glass pane in order to transfer stresses in in-plane direction between the glass pane and the metal framing by compression (see also system discussed in Section 2 and illustrated in Fig. 2b). The materials used for such an application require according to Ebert [31] *(i)* high compressive strength and high stiffness, *(ii)* constant properties between temperatures of −20 °C and +80 °C, *(iii)* significant lower surface hardness compared to glass, *(iv)* low tendency to creep under long-term loading, *(v)* low friction coefficient in contact with glass, *(vi)*

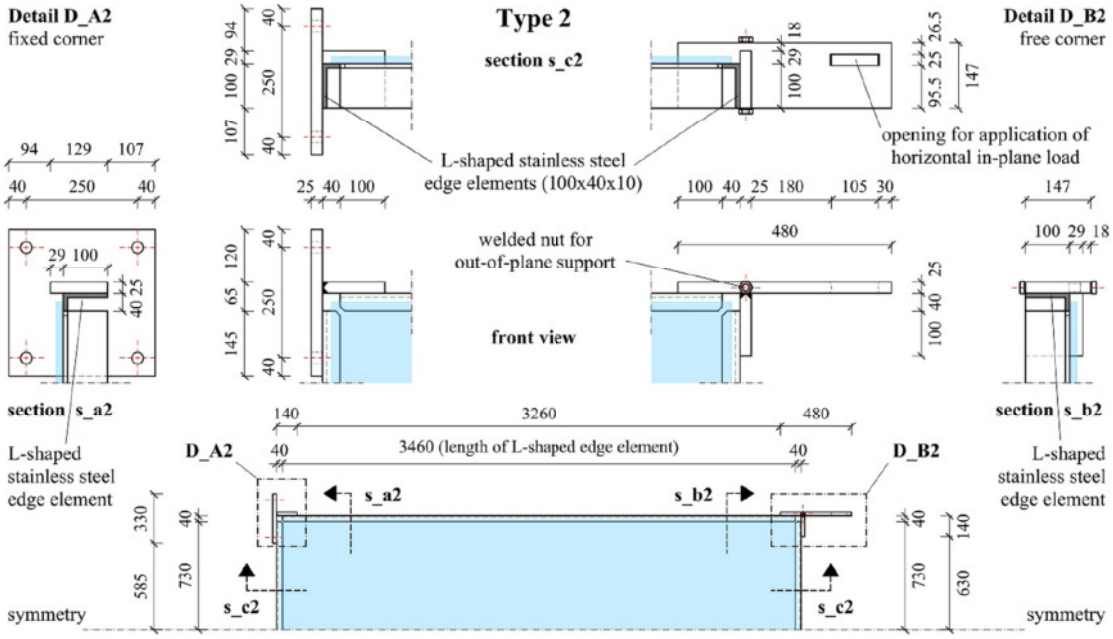

Fig. 5. Dimensions of the metal framing for the large-scale test specimen of Type 2 in [mm].

Table 2
Characteristics of the test specimen types for large-scale elements and mean values of the component values measured during assembling.

Specimen type	Characteristics of the test specimen type			Glass pane thickness [mm]	Adhesive thickness [mm]	L-shaped stainless steel edge element thickness [mm]	
	Glass pane	Adhesive	Grouting			Short leg	Long leg
Nominal value	–	–	–	10.0/13.52[a]	6.0/3.0[b]	10.0	10.0
Type 1A	10 mm TTG	Dow Corning 993 [18] A = 20 mm × 6 mm	Hilti HIT HY270 l = 100 mm, t = 10 mm	9.9	6.2	9.0	9.8
Type 1B	2 × 6 mm TTG with 1.52 mm PVB	Dow Corning 993 [18] A = 20 mm × 6 mm	Hilti HIT HY270 l = 100 mm, t = 10 mm	13.0	5.8	8.8	9.9
Type 2A	10 mm TTG	SikaFast-5221 NT [19] A = 20 mm × 3 mm	–	9.9	3.1	9.0	9.8
Type 2B	2 × 6 mm TTG with 1.52 mm PVB	SikaFast-5221 NT [19] A = 20 mm × 3 mm	–	13.1	3.1	9.2	9.8

[a] Different thicknesses for specimens with monolithic glass panes and specimens with laminated glass pares.
[b] Different thicknesses for specimens with silicone adhesive and specimens with acrylic adhesive.

resistance to UV-radiation, cleaning agents and corrosion, *(vii)* compatibility to other materials used for glass applications like interlayers and sealants and *(viii)* good workability and processability for shaping. Two types of materials have proved to sufficiently fulfil these requirements: *(a)* thermoplastics like the POM applied by Englhardt [4] for glass panes loaded by uniaxial compression and *(b)* injection grout like the products Hilti HIT-HY 50 investigated by Wellershoff [6] and by Mocibob [11] or Hilti HIT-HY 70 investigated by Bucak [32].

For the first category, the thermoplastics, results from extensive investigations under compressive loading on different materials (polyoxymethylene – POM, polyethylene terephthalate – PET, polyether ether ketone – PEEK, polyetherimide – PEI, polyamide – PA), some of them glass fibre reinforced, are presented by Ebert [31]. For the system of Type 1 investigated in this article, a solution with the resin-based injection grout Hilti HIT-HY 270 is chosen for the fact that it allows to counterbalance a possible edge offset in the case of laminated glass, since it is applied in a fluid state. This product is similar to the product Hilti HIT-HY 70, which is investigated at material level and at connection level by Kolany [33] along with the thermoplastic POM. At material level, prisms with a cross section of 10 mm × 10 mm and a height of 20 mm are tested under uniaxial compression to determine material properties as Young's modulus (~2500 MPa), Poisson's ratio (~0.40) and compressive strength (~75 MPa). At connection level, the test setup (see Fig. 6a) is designed in such a way, that the deformation of the grouting material is restrained in the direction of its width. Different dimensions of the laterally restrained grouting blocks are investigated. In Fig. 6b, the mean curve of the series with approximately the same block dimensions (80 mm long, 22 mm wide and 10 mm thick) as those used in the large-scale tests is illustrated. The value of 12 mm, which is provided in brackets, is the thickness of the glass pane. The diagram in Fig. 6b shows that significantly higher stresses can be transferred by the laterally restrained grouting. Furthermore, the obtained stress vs. strain relationship is almost linear. This is not the case for the uniaxially loaded prisms, which exhibit a non-linear behaviour after the occurrence of yielding. These observations are considered valid, despite the fact that the geometries of the specimens tested at material level and at connection level differ from each other (at material level the dimensions are chosen based on standards, while at connection level, the dimensions are based on the aimed application).

3.2. Design of the test setup and measurement instrumentation

Due to the constrains given in the laboratory for support and load application, the test setup is designed in a landscape format as illustrated in Fig. 7.

Fig. 8 illustrates the main dimensions of the test setup components and the distances between axes of fixing and loading along with a labelling of the main elements as a top view (Fig. 8a) and as a front view (Fig. 8b).

The setup is build on a 1.0 m thick prestressed concrete slab, which has an anchoring grid of 50 cm × 50 cm and allows for anchors loaded by a maximum of 500 kN each. The abutment block and the triangular structures for supporting the specimens as well as the four-column test rig for the in-plane shear load ($F_{s,i}$) and the abutment blocks for the in-plane compression load ($F_{n,i}$) and for the out-of-plane pressure load ($F_{p,o}$) are all fixed to the concrete slab.

The supports of the specimens simulate an element belonging to the bottom row of a façade as the one illustrated in Fig. 1. At one end (the left shorter side in Figs. 7 and 8) all six degrees of freedom are locked by connecting the two corner elements of the metal framing with four M24 8.8 bolts each to the abutment block. At the opposite end only the translational out-of-plane degree of freedom is locked with threaded rods which are connected to nuts welded on the corner elements of the metal framing. In order to provide only a negligible resistance in the other degrees of freedom, the rods have a diameter of 16 mm and a length of around 2000 mm. At the other end the threaded rods are

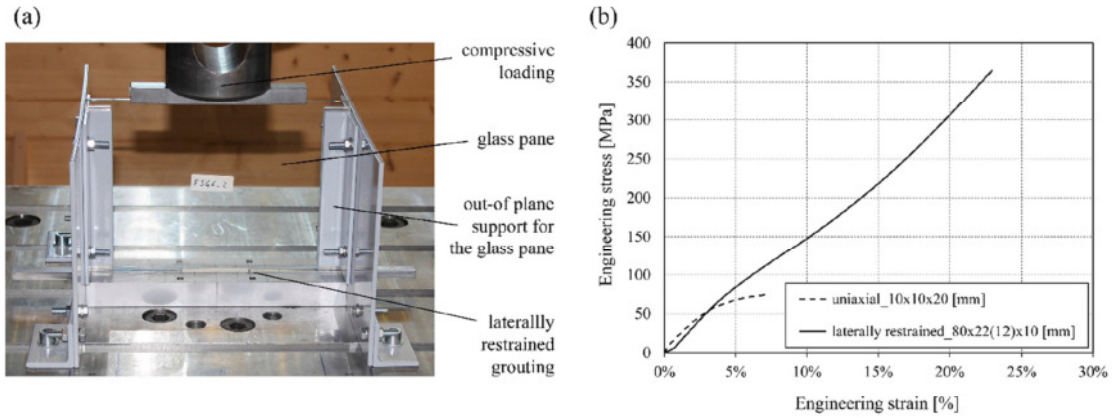

Fig. 6. Setup used for compression tests on laterally restrained prismatic specimens made of the applied resin-based injection grout (a) and comparison between results obtained from these tests to results from uniaxial compression tests on prismatic specimens (b).

connected to a bearing construction built of two connected triangles made of U-shaped profiles.

Loads in three different directions are applied on the specimens based on the expected in-plane and out-of-plane loading for an element belonging to a self-supporting transparent façade (see Fig. 1c). Hydraulic jacks for up to 1000 kN and allowing maximum strokes of 250 mm are used for the two applied in-plane loads, which act at the cantilevering end of the test specimens. The jack for the in-plane shear load ($F_{s,i}$) is fixed to the four-column test rig and acts vertically in the test setup at the intersection point between the middle plane of the glass pane and the middle plane of the corner element legs. A spherical pressure plate is used for the load introduction with the aim to avoid a rotational restraint of the specimen deformation by the load applying surface. Furthermore, a translational restraint is reduced by adding two thin polytetrafluoroethylene (PTFE) sheets between the bottom pressure plate surface and the top surface of the corner element.

The jack for the in-plane compression load ($F_{n,i}$) is connected to an abutment block. A distributing fin is used to apply the load into the longer legs of the two corner elements at the cantilevering end of the test specimens. Hinges are used to connect the hydraulic jack both to the abutment block and to the load-distributing fin. To avoid a loading of the test specimens with the dead weight of the jack, a cable is connected to the cylinder and diverted with a pulley to the basement through an anchoring hole, where a counterbalancing weight is holding the jack in equilibrium.

A hydraulic jack for up to 100 kN and allowing a maximum stroke of 250 mm is used for the out-of-plane load acting on the glass pane ($F_{p,o}$). At the end towards the test specimen the jack is connected to a structure made of formwork panels on which an air cushion is hanging. The air cushion, which is used to distribute the load from the hydraulic jack on the glass surface simulating wind suction, has a length of 3000 mm, a height of 1000 mm and a thickness of 150 mm. The connection to the hydraulic jack as well as the links to the test specimen allow the air cushion to rotate with the specimen loaded simultaneously by the in-plane shear load. At the other end the jack is fixed with a hinge to an abutment block. Similar to the jack for the in-plane compression load, also the dead weight of this one is counterbalanced with a weight hanging in the basement below the concrete slab.

In order to evaluate the structural behaviour of the glass-metal elements as a whole as well as of their single components, diverse measurement instrumentation is used. Additionally to the recorded loads and displacements of the hydraulic jacks ($F_{s,i}$ & $D_{s,i}$, $F_{n,i}$ & $D_{n,i}$ and

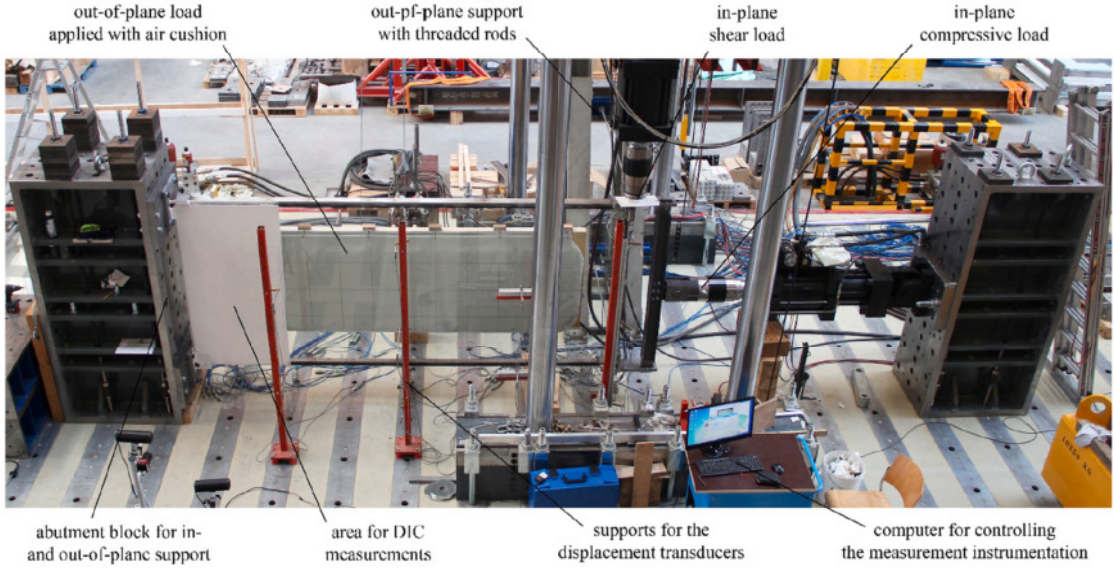

Fig. 7. Overview of the setup for testing the large-scale specimens.

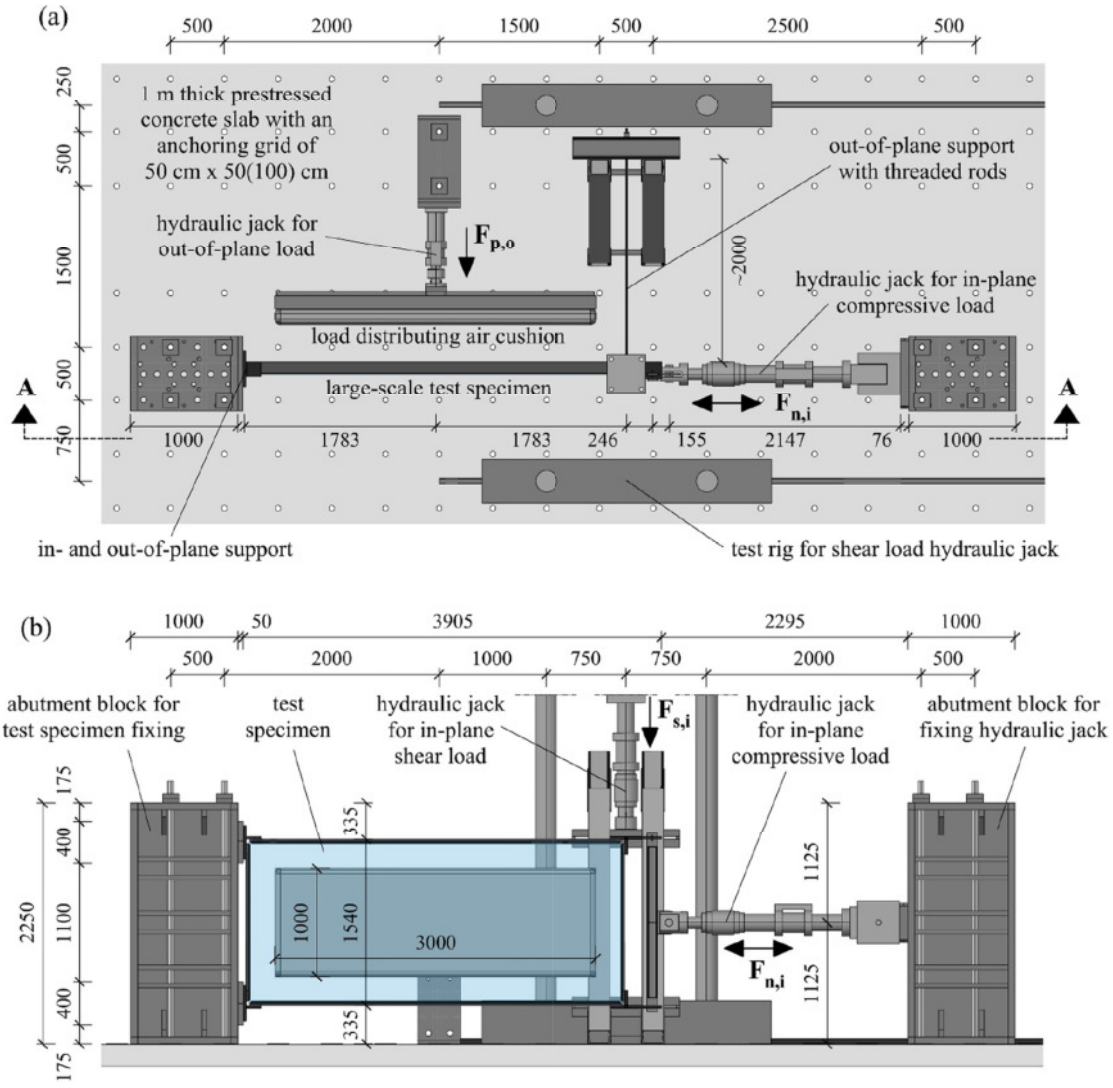

Fig. 8. Main dimensions of the setup in [mm] for testing the large-scale specimens illustrated in a top view (a) and a front view (b).

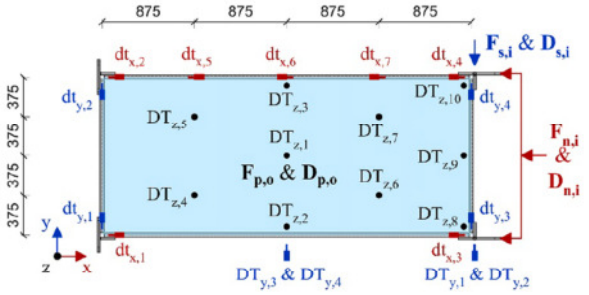

Fig. 9. Positions of the measurement instrumentation for recording global deformations of the glass-metal elements (labelled with upper case letters, dimensions in [mm]) as well as the local relative displacements between metal framing and glass pane (labelled with lower case letters).

$F_{p,o}$ & $D_{p,o}$ in Fig. 9), most of the performed measurements during testing are done with linear variable differential transformers (LVDT), which are further addressed as displacement transducers (DT) in this article. The schematic position of the displacement transducers is illustrated in Fig. 9. The transducers measuring absolute global deformations are labelled with upper case letters (e.g. $DT_{z,1}$), while those recording relative deformations between the metal framing and the glass pane are labelled with lower case letters (e.g. $dt_{x,1}$). Ten displacement transducers ($DT_{z,1}$ to $DT_{z,10}$) are positioned on the glass pane surface to capture the shape of out-of-plane displacements due to surface loading or due to plate buckling. Four displacement transducers ($DT_{y,1}$ to $DT_{y,4}$) measure the distance between the ground and the bottom edge element in order to capture an eventual twisting of this element around the x-axis. The in-plane relative displacements between the glass pane and the metal framing are measured primarily near the corners since the largest values are expected in these areas ($dt_{x,1}$ to $dt_{x,4}$ and $dt_{y,1}$ to $dt_{y,4}$). These displacement transducers are positioned in a distance of around 70 mm from the glass pane corners for the system of Type 1 and around 120 mm for the system of Type 2. For the system of Type 2, additional transducers, which are not evaluated within this paper, are applied along the top edge element ($dt_{x,5}$ to $dt_{x,7}$).

Additionally, displacement transducers for the relative displacements in z-direction between the glass pane and the metal framing, strain gauge rosettes near selected corners of the glass pane and a digital image correlation (DIC) system on a predefined area are used.

However, these results are not evaluated in this article and can be found in Silvestru [28].

3.3. Loading scenarios

The aim of the applied loading programme is to obtain from the reduced number of test specimens an extended amount of information and data on the structural behaviour of the glass-metal elements. For all four specimens, load scenarios with single loads increased up to a certain value and, afterwards, scenarios with load combinations with one or two loads kept constant and the shear load increased up to a specific value are performed. Finally, the two specimens with laminated glass panes (Type 1B and Type 2B) are tested to failure under shear loading. The primary focus in the investigations is set on the behaviour of the large-scale multi-component elements under in-plane shear loading as well as on the influence which additional loadings (in-plane axial loading and out-of-plane surface loading) have on this behaviour.

For the in-plane axial loading ($F_{n,i}$) forces up to 40 kN are applied covering an eventual dead weight of additional elements or of a small glass roof. Loads from massive roofs or slabs are not expected to be supported by the investigated system. Since the global and relative displacements resulting under these loads are extremely small compared to those resulting under the applied in-plane shear loads and out-of-plane loads, the results including in-plane axial loads are not discussed in this article. For the out-of-plane surface loading ($F_{p,o}$) forces up to 15 kN are applied, corresponding to approximate surface loads of up to 3.0 kPa. For the scenarios with combined loading directions, the in-plane shear loading ($F_{s,i}$) is increased up to 30 kN. In the case of the failure tests, the in-plane shear loading is applied displacement-controlled. Different rates are used for the two systems based on expected final displacements: *(i)* 2 mm/min for Type 1B and *(ii)* 0.5 mm/min until reaching a load of 100 kN and 1 mm/min after passing this load for Type 2B. In Section 4 of this article only results for selected loading scenarios are presented and discussed. Results from additional loading scenarios can be found in Silvestru [28].

3.4. Model characteristics for finite element simulations

In addition to the experimental investigations, the structural behaviour of the novel glass-metal elements is also analysed by non-linear finite element simulations. The developed models exhibit some particular characteristics regarding material properties and contact definitions which are presented in this subsection.

Linear-elastic material models are used for the glass, the interlayer and the grouting. The Young's modulus of the interlayer is assumed according to the value proposed by Wellershoff [6] for wind loading for PVB. For the grouting Kolany [33] investigates more detailed material models including plasticity and creep effects. However, based on the laterally restrained situation (see also Section 3.1.2), the linear-elastic model is considered sufficiently precise. For the stainless steel used for the edge elements and the structural steel used for the corner elements, plastic properties are implemented by providing additional to the Young's modulus and the Poisson's ratio yielding stress values at given plastic strains. In the case of the adhesives, additional to linear-elastic models, the hyperelastic Mooney-Rivlin model proposed in Silvestru et al. [29] is used for the silicone, while for the acrylic the strain rate dependent plastic model without porosity introduced in Silvestru et al. [30] is applied. The yielding stress values proposed in Silvestru et al. [30] for the acrylic are reduced by 30% to obtain a suitable fit. This reduction is assumed to cover the influence of the given material porosity of the acrylic adhesive. Table 3 summarizes the input values for the material properties used in the finite element simulations.

The used mesh discretisation, finer in the corners and getting coarser towards the centre of the elements, is illustrated in Fig. 10. A minimum of four elements across their thickness as well as across their width is used for the adhesives and for the grouting blocks. All components are modelled with second order solid elements. In the models of Type 1 elements of type C3D20 according to Abaqus [36] are used for the glass pane, the interlayer, the metal framing and the grouting blocks, while the silicone adhesive is modelled with elements of type C3D20H because of the incompressibility of the material. In the models of Type 2 all components, including the acrylic adhesive, are modelled with elements of type C3D20.

Tie constraints are used to model the contact between the two adhesives and the substrates. The adhesives provide always the slave surfaces. The same type of constraint is used between the corner elements and the edge elements, simulating the welded connection, as well as between the glass panes and the interlayer in the case of the models with laminated glass. Different assumptions are made for the contact of the grouting blocks to the framing and to the glass panes. Between the grout and the stainless steel, a certain bonding is given and, therefore, tie constraints are applied between these surfaces. Between the glass and the grout the following interaction properties are defined: *(i)* in normal direction contact occurs when the two components are pushed together (hard contact), while in the case of a movement away from each other, separation is allowed; *(ii)* in tangential direction a friction coefficient of $\mu = 0.2$ is assumed.

The boundary conditions and the load application used in the models are illustrated in Fig. 10. The investigated loads are applied as concentrated forces on defined reference points, which are connected with rigid body constraints to surfaces of the glass-metal elements in accordance with the experimental test setup. For the glass pane thickness and for the thickness of the L-shaped stainless steel edge elements, the real measured values provided in Table 2 are used in the finite element simulations.

For stability simulations with finite element software both Luible [3] and Englhardt [4] state that non-linear analysis on systems with initial geometric imperfections defined based on eigenmodes should be carried out. The initial geometric imperfections are indispensable in the case of structural elements with both symmetrical geometry and symmetrical loading. In the case of the investigated glass-metal elements, the loading is applied centric to the glass pane, but the framing is positioned on one side of the glass pane, towards the inside of the façade. Due to this non-symmetric configuration, the influence of initial geometric imperfections on the results is negligible and, therefore, a non-linear analysis without initial geometric imperfections is sufficient for most loading scenarios. The simulation results shown in this article are obtained without initial geometric imperfections. A comparison between simulation results with and without initial geometric imperfections for the failure tests and the observed insignificant differences can be found in Silvestru [28].

4. Results and discussion

Results from three different loading scenarios are presented and discussed within this article based on global deformations of the glass-metal elements as well as on relative displacements between the glass pane and the metal framing: *(i)* out-of-plane loading alone (Section 4.1), *(ii)* combined out-of-plane loading and in-plane shear loading (Section 4.2) and *(iii)* in-plane shear loading alone until failure (Section 4.3). For the specimens tested until failure, also the failure modes from the experiments and selected stress values from the finite element simulations are discussed. The results for the two investigated configurations are discussed in parallel to allow a better comparison. The diagrams and illustrations for the system of Type 1 are shown in Figs. 11a–22a, while those for the system of Type 2 are shown in Figs. 11b–22b.

4.1. Results under out-of-plane loading alone

For out-of-plane loading alone, the results from the series run up to the maximum load of 15 kN are evaluated in this subsection. Figs. 11

Table 3
Material properties used in the finite element simulations.

Material	Model type	Elastic properties		Plastic properties			
		Young's modulus [MPa]	Poisson's ratio [–]	Yield stress [MPa]	Plastic strain [%]	Tensile strength [MPa]	Plastic strain [%]
Glass	Linear-elastic	70,000	0.23	–	–	–	–
Interlayer	Linear-elastic	1.2	0.49	–	–	–	–
Stainless steel[a]	Plastic	200,000	0.30	240	0%	600	40%
Structural steel[a]	Plastic	210,000	0.30	345	0%	550	20%
Grout	Linear-elastic	2500	0.40	–	–	–	–
Silicone adhesive	Linear-elastic	2.4	0.49	–	–	–	–
	Hyperelastic	Mooney-Rivlin model proposed by Silvestru et al. [29] with c_{10} = 0.333349 MPa and c_{01} = 0.010943 MPa					
Acrylic adhesive	Linear-elastic	250	0.47	–	–	–	–
	Plastic	250	0.47	Adapted strain rate dependent plastic model proposed by Silvestru et al. [30]			

[a] The values for the elastic and plastic properties are chosen based on [34] for the stainless steel and based on [35] for the structural steel.

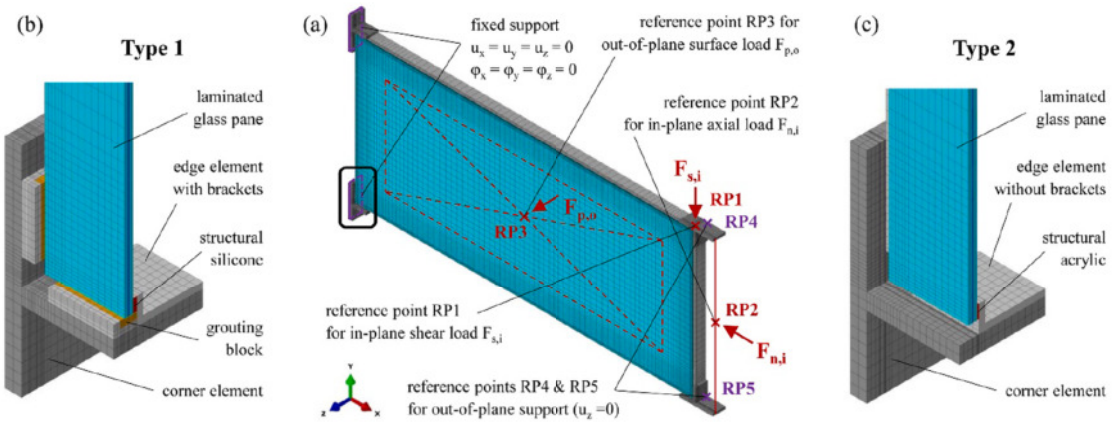

Fig. 10. Characteristics of the finite element model: (a) global mesh discretisation, boundary conditions and reference points for applied loads and displacements; (b) detailed view of a fixed corner for the system of Type 1; (c) detailed view of a fixed corner for the system of Type 2.

and 12 show the development of the out-of-plane displacements of the glass pane along one of the diagonals (the diagonal which would be compressed under shear loading in the test setup) in its middle and in the two quarter-points. In the middle of the glass pane ($DT_{z,1}$) displacements of up to 37 mm (~L/40) are reached in the case of the specimens of Type 1 and of up to 30 mm (~L/50) for the specimens of Type 2. Because the out-of-plane support at the cantilevering end is softer than that at the fixed end, the deformation shapes are not completely symmetric (compare $DT_{z,4}$ to $DT_{z,7}$). By comparing the specimens with different design configurations to each other, it can be observed that those with acrylic adhesive joints behave, as expected, slightly stiffer than those with silicone adhesive joints. The grouting used for specimens of Type 1 near the glass pane corners has no significant influence on the system behaviour under this type of loading.

By comparing the displacements measured for the specimens, which have the same configuration, once with monolithic glass (10 mm) and once with laminated glass (2 × 6 mm), it can be observed that the maximum displacements are almost the same (see Fig. 11). However, there are differences in the development of the curves. The loading (thicker curves in Figs. 11–14) and the unloading paths (thinner curves

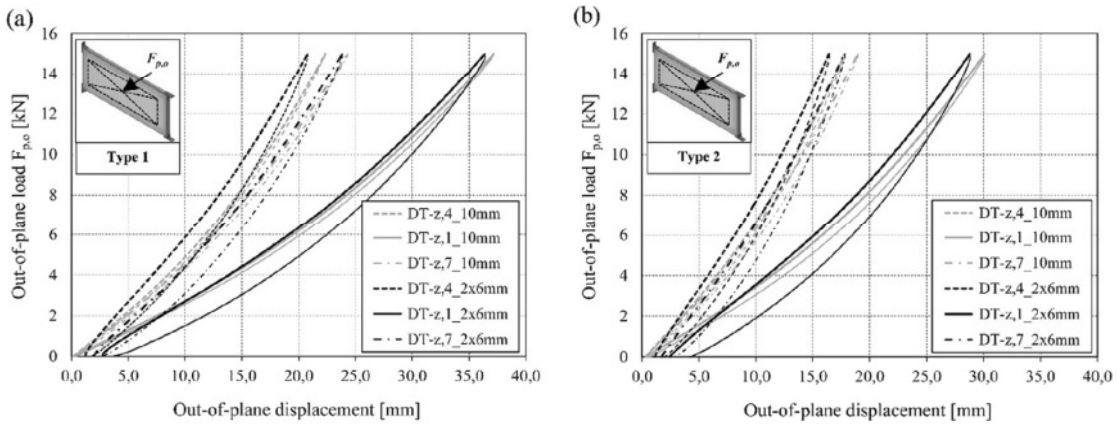

Fig. 11. Out-of-plane displacements measured along one diagonal for (a) the specimens of Type 1 with monolithic glass panes (Type 1A) and with laminated glass panes (Type 1B) and for (b) the specimens of Type 2 with monolithic glass panes (Type 2A) and with laminated glass panes (Type 2B).

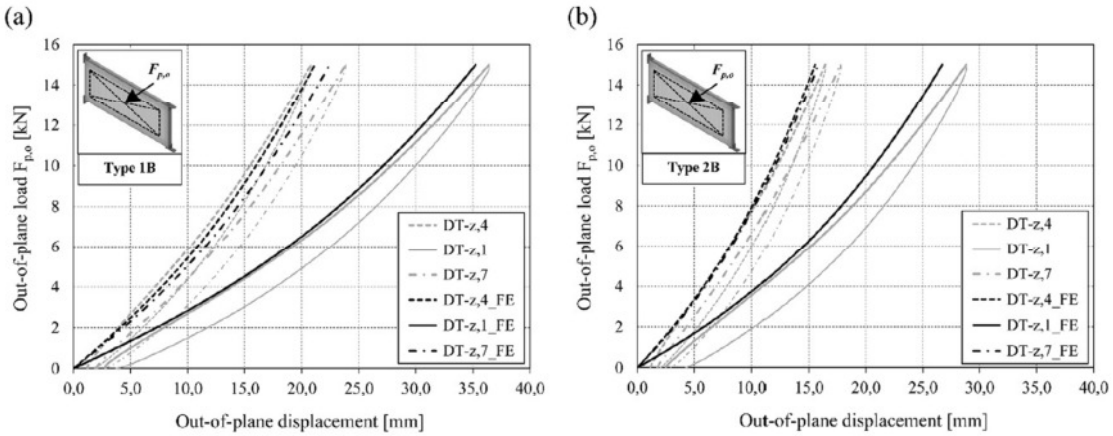

Fig. 12. Comparison of experimental and simulation results for out-of-plane displacements along one diagonal of the glass pane for specimens Type 1B (a) and Type 2B (b) under out-of-plane surface loading.

in Figs. 11–14) are almost the same for the specimens with monolithic glass panes. In the case of the specimens with laminated glass panes, discrepancies between the loading and the unloading path can be noticed. This aspect results due to the viscous material behaviour of the 1.52 mm thick interlayer used to laminate the glass panes. Furthermore, the behaviour of the interlayer is also the reason for the incomplete or delayed recovery after unloading.

The diagrams plotted in Fig. 12 show a good agreement between the results obtained from the finite element (FE) simulations and those from the experimental tests for the out-of-plane displacements of the glass panes in the case of the specimens with laminated glass.

In Fig. 13, the global in-plane displacements measured in the middle ($DT_{y,3}$ and $DT_{y,4}$) and at the free end ($DT_{y,1}$ and $DT_{y,2}$) of the specimens with laminated glass panes are evaluated. At the free end almost no displacements are observed. In the middle of the elements both measurement points on the frame profile move towards the centre of the glass pane. The displacements of the point near the glass pane ($DT_{y,3}$) are smaller than those of the point at the interior edge of the frame profile ($DT_{y,4}$), which means that the out-of-plane loading causes a rotation of the edge elements around their longitudinal axis. The fact that this rotation is more pronounced in the case of the specimens with acrylic adhesive confirms the expected stronger composite action for this type of loading. From Fig. 13 a relatively good agreement between FE-simulation and experimental results can be observed also for the global in-plane displacements.

4.2. Results under combined out-of-plane and in-plane loading

For the series under combined out-of-plane and in-plane loading, an out-of-plane load ($F_{p,o}$) of 10 kN is first applied and then the in-plane shear load is raised up to 30 kN. The out-of-plane displacements along the compressed diagonal of the glass pane, which are plotted in Fig. 14 for the specimens with laminated glass, show for both specimen types that the larger share results from the out-of-plane loading. Therefore, it is expected that the additional out-of-plane load would lead to an earlier plate buckling of the glass pane if the in-plane shear load would be further increased, compared to the case of a loading with in-plane shear load alone.

The out-of-plane displacements obtained from FE-simulations are in a relatively good agreement with those from the experimental tests in terms of maximum values. However, it can be noticed that the experimentally determined curves show non-linear developments with a smaller inclination at the beginning of in-plane loading. This occurs probably due to the resilience of the air cushion used for out-of-plane loading in the tests, which is not considered in the simulation.

4.3. Results under in-plane shear loading until failure for the specimens with laminated glass panes

For these loading series, the failure modes from the tests, selected global and relative displacements both from the tests and the

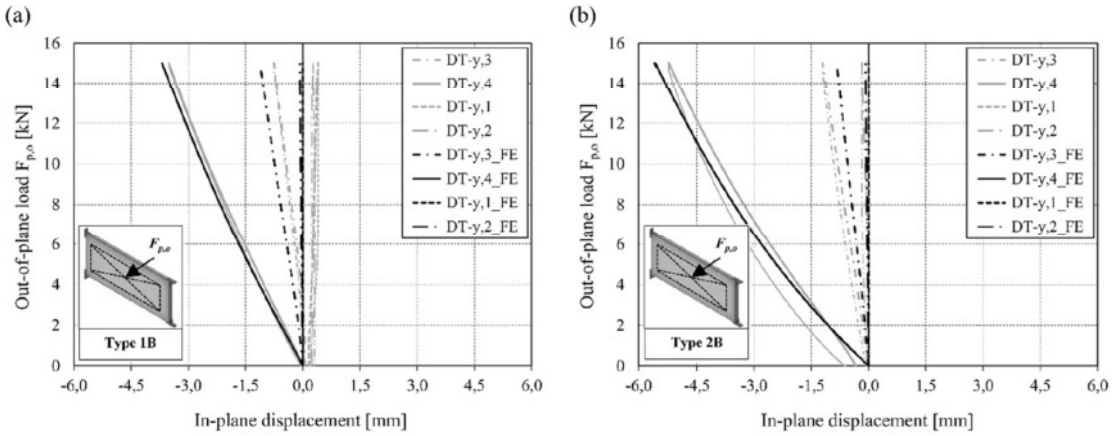

Fig. 13. Comparison of experimental and simulation results for in-plane displacements in the middle and at the free end of the bottom frame profile for specimens Type 1B (a) and Type 2B (b) under out-of-plane surface loading.

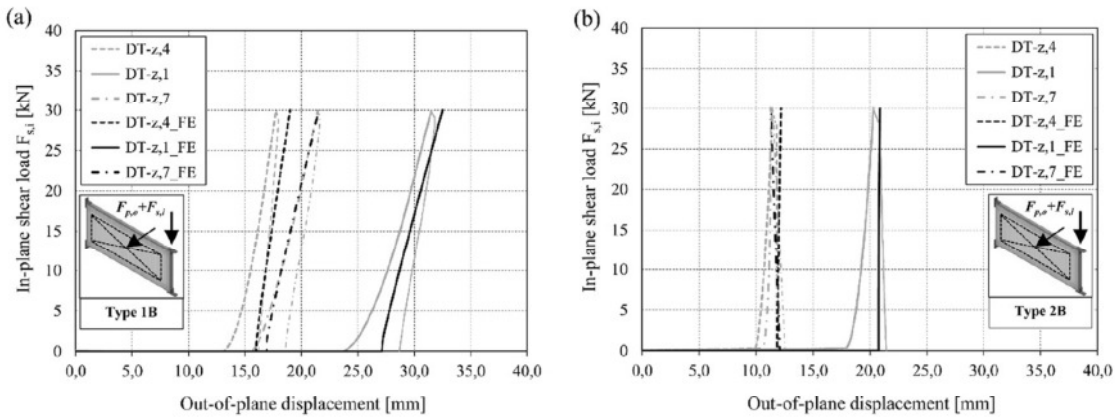

Fig. 14. Comparison of experimental and simulation results for out-of-plane displacements along the compressed diagonal of the glass pane for specimens Type 1B (a) and Type 2B (b) under combined out-of-plane surface loading and in-plane shear loading.

simulations as well as selected stress values from the simulations are evaluated. Fig. 15 shows the two specimens with laminated glass panes tested until failure, before loading (Fig. 15a for Type 1B and Fig. 15d for Type 2B, respectively), during loading, shortly before failure (Fig. 15b and Fig. 15e, respectively) and immediately after failure (Fig. 15c and Fig. 15f, respectively). By comparing the reflections in the glass panes for the test specimens before loading and the loaded specimens shortly before failure, distortions can be observed in the loaded state, especially for the specimen Type 1B. This indicates the occurring plate buckling.

The failure is recorded at an in-plane shear load of ~93 kN for the system with silicone adhesive and grouting and of ~133 kN for the system with acrylic adhesive. For the first system, the failure is initiated by cracks in the adhesive along the top edge and is followed immediately by a glass failure near the corner on which the load is applied. Based on the video recording of the test, it can be observed that the crack in the silicone adhesive initiates approximately in the centre of the top edge and then propagates towards the loaded corner. In the moment the crack reaches the corner, the glass is not bonded anymore to the framing in this area, probably hits the bracket for grouting block enclosure and glass breakage results. In the case of the specimen Type 2B, the failure is caused by mixed cohesive failure within the acrylic adhesive and loss of adhesion to the glass substrate. However, the adhesive already starts to yield locally at around 50 kN with the consequence of significant stiffness reduction of the whole system, since the composite action is decreasing and the glass pane cannot be activated anymore as a shear panel to the same extent. Although there is an acoustically perceptible shock in the moment of ultimate failure, no glass breakage occurs in the case of the specimen Type 2B (see Figs. 15f and 16b). This is due to the fact, that there are no stainless steel brackets in the corners to block the movement of the glass pane after the shock, as it is the case for specimen Type 1B. Based on the video recording of the test, it can be observed that the failure in the acrylic adhesive is initiated in the top left corner (this corner is under tension) and propagates along the top edge towards the right top corner. However, the ultimate failure, after which the load drops, occurs when the adhesive fails along the right glass edge.

After failure both systems get significantly softer, which can be recognized by the way the glass-metal elements are hanging under their dead weights (see Fig. 16). Without the intact glass pane activated as a compression diagonal or as a shear panel the filigree metal framing has

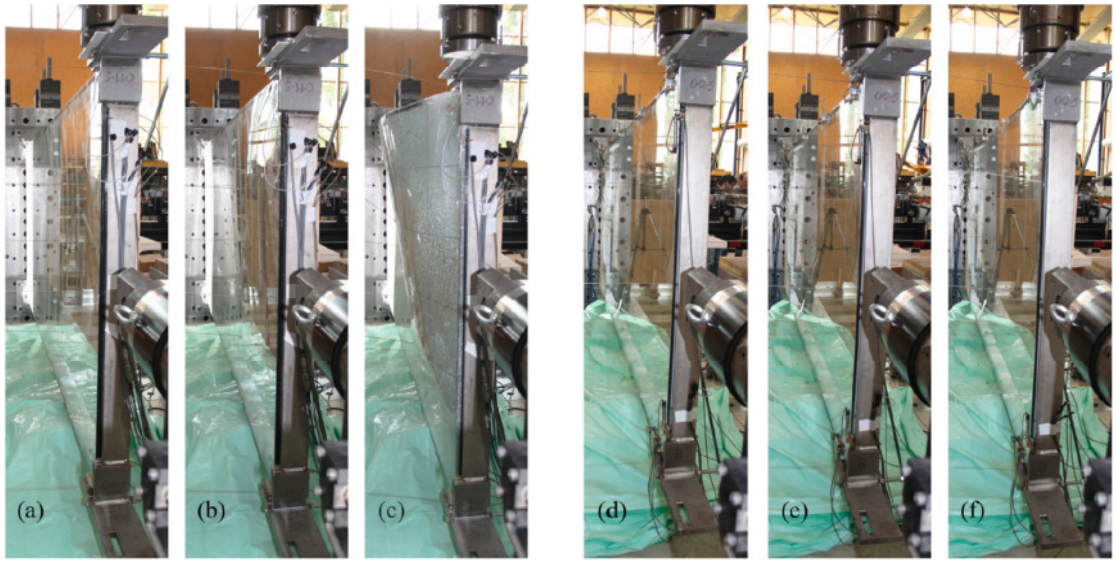

Fig. 15. Different stages of testing for specimen Type 1B – (a) before loading, (b) shortly before failure and (c) after failure – and for specimen Type 2B – (d) before loading, (e) shortly before failure and (f) after failure.

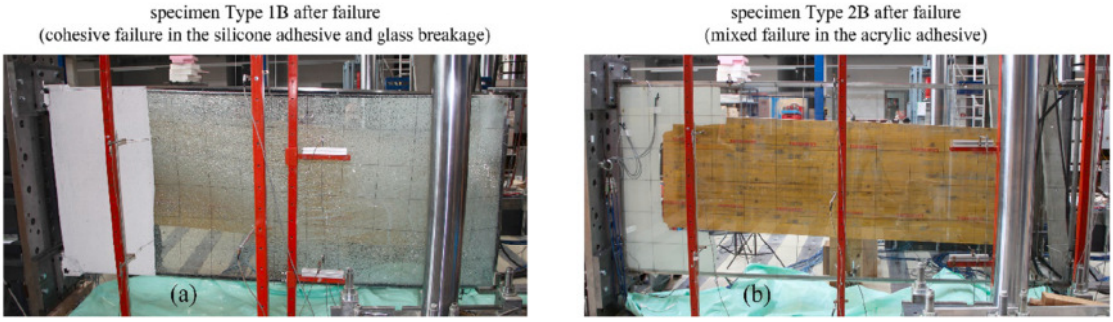

Fig. 16. Front views of specimen Type 1B (a) and of specimen Type 2B (b) after failure.

a low in-plane stiffness.

In the case of the specimen Type 1B, the adhesive joint along the top edge element is cracked over almost its entire length at the moment of glass breakage (see Fig. 17a). The failure pattern of the silicone adhesive is entirely cohesive. In the case of specimen Type 2B, the failure of the acrylic adhesive can be observed near all four corners as well as on significant parts along the edges. The mixed failure pattern along the top edge is illustrated in Fig. 17b. However, at the end of testing there are still parts of the adhesive joint with an effective bonding which prevents the glass pane from falling to the ground (see also Fig. 16b).

The diagrams in Fig. 18 show the relationships between the applied in-plane shear load and the in-plane displacement in load direction for the two different specimens. Additionally to the continuous curves obtained from the experimental tests, curves determined from the non-linear simulations with different material models for the adhesives are plotted. In the case of specimen Type 1B, a relatively good agreement between simulation results and experimental ones is reached already with the linear-elastic material model. This indicates, that the non-linearity of the curves results to a high extent due to yielding in the metal framing. For specimen Type 2B, a good agreement is provided with the linear-elastic material model only up to a load of around 50 kN. Above this value, the acrylic adhesive begins to yield and the in-plane stiffness of the glass-metal elements starts to decrease.

The use of the hyperelastic material model Mooney-Rivlin for the silicone adhesive in the case of the specimen Type 1B leads to a slightly better agreement between simulation and experimental results. For the specimen Type 2B, the addition of plasticity to the material properties of the acrylic adhesive leads to an improvement of the simulation results, since the yielding behaviour of the adhesive and implicitly the decrease in in-plane stiffness can be reproduced. However, it is observed from Fig. 18b that the yielding starts in the model a little delayed and therefore the loads from the tests are overestimated after yielding. Based on the investigations discussed in Silvestru et al. [30] for the acrylic adhesive, these discrepancies are considered to be caused by the porosity of the acrylic adhesive and by related cavitation effects. In order to consider these properties in absence of a more suitable material model, the strain rate dependent plastic model proposed in Silvestru et al. [30] is modified by reducing the strain rate dependent yield stresses by 30%. As shown by the results in Fig. 18b as well as in Fig. 20b, this procedure leads to a relatively good agreement between simulation and experimental results. Nevertheless, thorough investigations aiming at developing a generally suitable plastic model taking existing voids, void nucleation and coalescence into account are recommended for the acrylic adhesive in future research.

Fig. 19 shows the development of the out-of-plane displacements along the compressed diagonal of the glass pane in its middle and in the two quarter-points. It can be noticed, that the occurring displacements are higher in the case of the system with silicone adhesive and grouting. Furthermore, it can be observed that the simulations deliver relatively good qualitative results, but quantitatively the displacements from the simulations are generally larger than those from the experiments.

The relative in-plane displacements between the glass pane and the metal framing in the two corners belonging to the top frame profile are illustrated in Fig. 20. For the system with silicone adhesive and grouting, significantly higher displacements occur in the corner under tension, especially in x-direction. While in the top right corner (compression), values of up to 1.5 mm are reached (~15% compression of the grouting), values of up to 10 mm are reached in the top left corner (tension), which correspond to ~160% shear displacement within the adhesive joint. In the case of the system with acrylic adhesive, only small differences are noticed between the relative displacements recorded in the two corners belonging to the top frame profile. The maximum measured values of up to 7 mm correspond to ~230% shear displacement within the adhesive joint. An evaluation of the simulation results in terms of the behaviour of the intermediary materials is carried out, by comparing the relative in-plane displacements between glass pane and metal framing. A good agreement can be noticed based on the curves plotted in the diagrams from Fig. 20.

The maximum principal stresses in the glass panes before failure of the elements are significantly higher in the case of the system with silicone adhesive and grouting. This is due to the concentrated stress transfer from the metal framing to the glass pane through the grouting blocks. The maximum stress of 125 MPa, which is slightly higher than the characteristic strength value for thermally toughened glass given in standards (e.g. [37]) with 120 MPa, occurs in the simulation in the loaded corner, directly near the location of the grouting as shown in Fig. 21a. Significantly lower stresses are reached over the surface of the glass pane, where bulges from out-of-plane deformations are located.

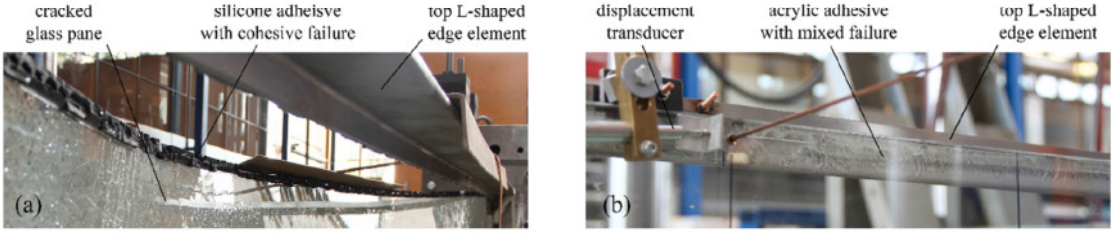

Fig. 17. Detailed views of the crack patterns in the adhesives along the top framing profile for specimen Type 1B (a) and for specimen Type 2B (b).

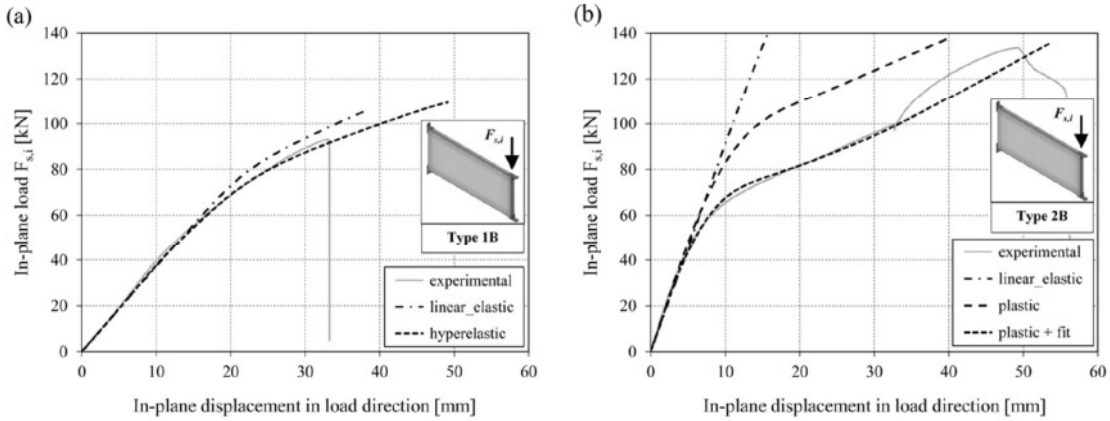

Fig. 18. In-plane shear load vs. in-plane displacement of the hydraulic jack during the failure tests for specimens Type 1B (a) and Type 2B (b) compared to the in-plane displacements of reference point RP1 from the finite element simulations of these tests.

The principal stresses over the glass pane surface are even lower in the case of the system with acrylic adhesive and there are no peaks in the area of the loaded corner of this element (see Fig. 21b). The maximum principal stress of 71 MPa occurs on the back side of the glass pane near the fixed corner belonging to the tensioned diagonal.

The two different stress transfer methods between the metal framing and the glass pane have also an influence on the stresses in the framing as shown by the contour plots of the Mises stress distribution in Fig. 22. In the case of the system with silicone adhesive and grouting, the stresses are mainly transferred by compression over the grouting in the two corners belonging to the compressed diagonal. As a consequence, high stresses of up to 449 MPa result in these two corner elements at an in-plane shear load of 90 kN and lead to yielding of the given structural steel type (S355). In the case of the system with acrylic adhesive, the stresses are transferred by shear, which leads to local stress peaks in the corner elements at the border of the welded joints. Regarding the edge elements, different stress distributions can be observed as well for the two systems. In the case of the simulation for the specimen Type 1B, higher stresses can be observed only in the longer top edge element, which functions as a tie member. For the specimen Type 2B, the simulation reveals a more uniform distribution with increased stresses in both longer edge elements towards their fixed end.

Based on the finite element simulations also stresses in the adhesives can be evaluated. In the case of the system of Type 1, the highest values of the maximum principal stresses in the silicone adhesive (~4.6 MPa) are occurring near the fixed corner of the tensioned diagonal of the glass pane, where no stresses can be transferred by the grouting. These values should not be regarded as distributed stresses, but as stress peaks in the direct vicinity of the substrate materials. Furthermore, high stress values are also noticed along the top edge element, which is in agreement with the area of crack initiation. In the case of the system of Type 2, high values for Mises stresses in the acrylic adhesive (up to ~ 20 MPa) are occurring in all four corners and confirm yielding in these areas.

5. Conclusions

The results discussed in this article substantiate that adhesively bonded glass-metal elements with composite structural behaviour show a high potential for future application in transparent facades. The two novel configurations can bear, additionally to out-of-plane loads as structural glazing systems already do, also significant in-plane shear loads. Therefore, the introduced configurations could be used for future self-supporting building skins as for example the exterior layer of a double-skin façade. In the case of both investigated systems, for the chosen dimensions of the different components, the weakest component which initiates the failure turns out to be the adhesive. Although the system with acrylic adhesive bonding reaches a 1.5 times higher failure load under shear than the system with silicone adhesive bonding and grouting, the second one allows for a better activation of the glass pane.

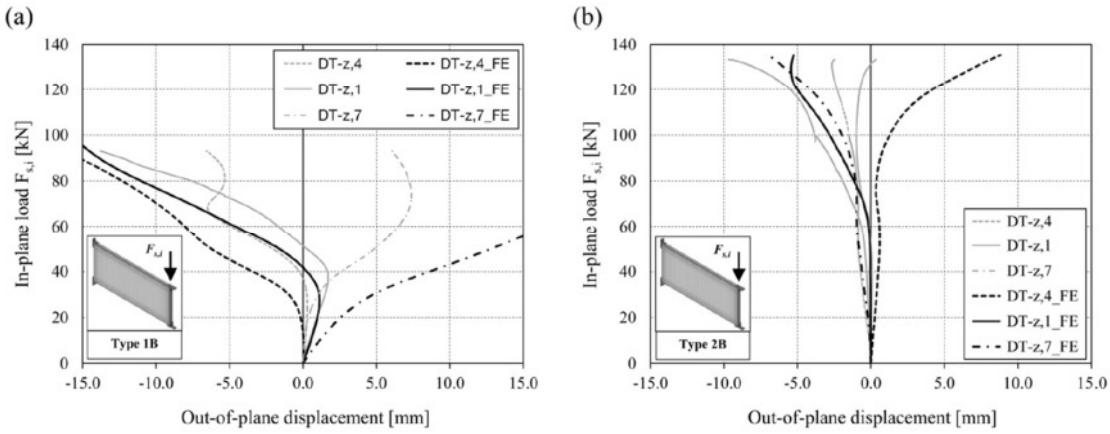

Fig. 19. Out-of-plane displacements of the glass panes along the compressed diagonals measured during the failure tests compared to values obtained from finite element simulations of these tests for specimens Type 1B (a) and Type 2B (b).

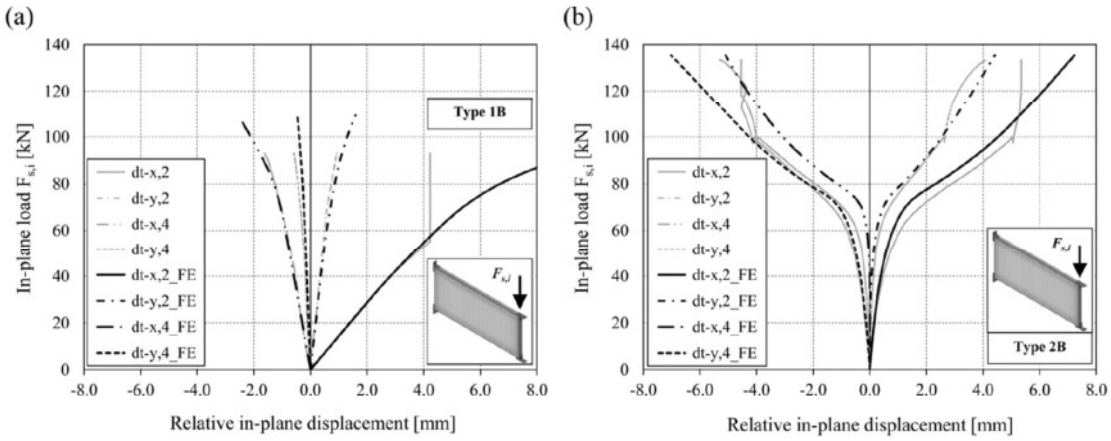

Fig. 20. Relative in-plane displacements between glass pane and metal framing obtained from the experimental tests and from the FE simulations for specimen Type 1B (a) and for specimen Type 2B (b) in the two corners belonging to the top frame profile.

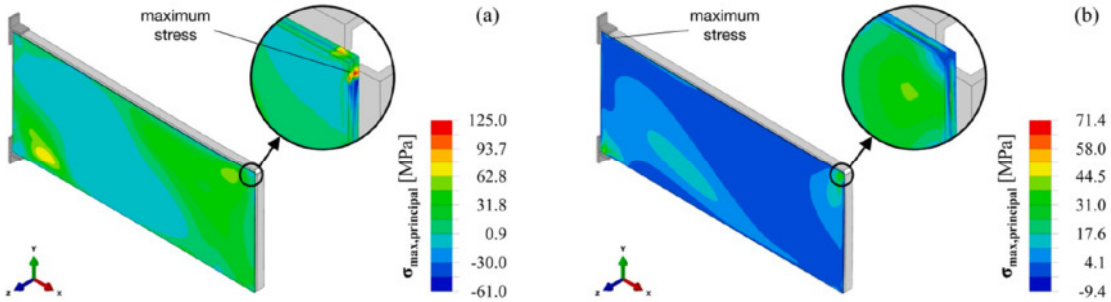

Fig. 21. Maximum principal stresses in the glass panes obtained from the finite element simulations for specimen Type 1B at an in-plane shear load of 90 kN (a) and for specimen Type 2B at an in-plane shear load of 130 kN (b).

This is due to the fact that the stiffness of the system with acrylic adhesive decreases significantly after yielding of the acrylic. Furthermore, this aspect is substantiated by the larger out-of-plane displacements measured for the system with silicone adhesive and grouting under shear loading, which indicate a plate buckling of the glass pane.

The system with silicone adhesive and grouting has the advantage of using intermediary materials which already have technical approvals for related applications. Furthermore, the failure of this system is announced by large out-of-plane deformations of the glass pane. For structural design, relatively simple material models can lead to good predictions of the system stiffness and of occurring displacements. Limitations for this system could result from creeping or plastic deformations of the grouting material (these aspects are assessed by Kolany [33]). The system with acrylic adhesive has the advantages of a perimetrical more uniform transfer of the stresses in in-plane direction between glass pane and metal framing as well as of a higher stiffness until the adhesive starts to yield. The limitations for this configuration result from finding an alternative adequate adhesive, since the applied acrylic adhesive does not have a technical approval for the use in facades and its mechanical properties are known to degrade with

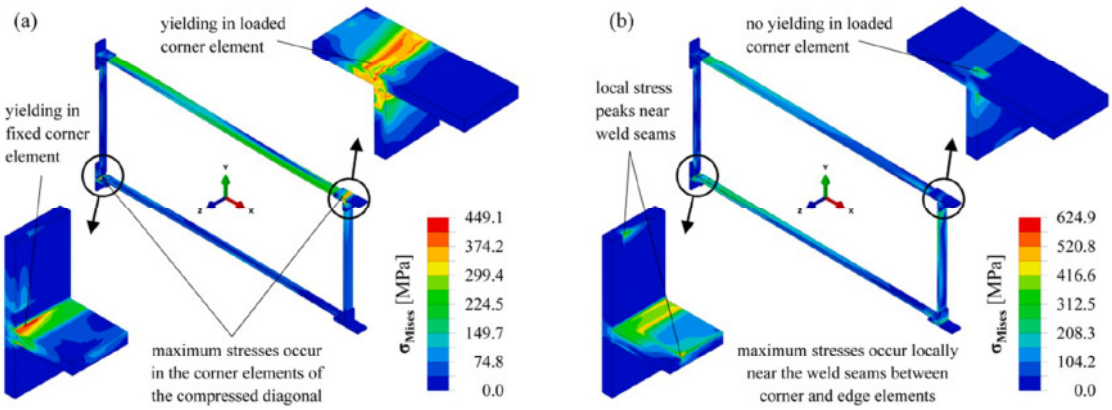

Fig. 22. Mises stresses resulting in the metal framing obtained from finite element simulations for specimen Type 1B at an in-plane shear load of 90 kN (a) and for specimen Type 2B at an in-plane shear load of 130 kN (b).

increasing temperature.

Considering the structural potential of the investigated glass-metal elements with composite structural behaviour, future research should focus on the behaviour of such elements during thermal cycles, the optimization of the connections between several elements, elaboration of redundancy concepts for systems with several glass-metal elements and the development of prototype façade elements based on the introduced configurations. Moreover, investigations should be carried out in order to find more adequate adhesives for the configuration with adhesive bonding alone, especially regarding the durability of candidate adhesives to environmental agents. Furthermore, despite the increasing use of finite element software in structural design, the development of analytical methods for designing glass-metal elements with composite structural behaviour could be as well addressed in future research.

Declaration of Competing Interest

The authors declare that they have no known competing financial interests or personal relationships that could have appeared to influence the work reported in this paper.

Acknowledgements

This research has been carried out at Graz University of Technology as part of the FFG research project no. 838561. Furthermore, results from the completed doctoral thesis of the first author [28] as well as of the doctoral thesis in progress of the second author [33] are included in this article. The authors would like to acknowledge the collaboration with Waagner-Biro Stahlbau AG on this research project as well as the financial support from the Austrian Research Promotion Agency (FFG) and from Waagner-Biro Stahlbau AG. Furthermore, the authors acknowledge the support of Sika Österreich GmbH by providing the acrylic adhesive as well as the support of both Dow Corning Europe S.A. (currently Dow Silicones Belgium SPRL) and Sika Services AG for valuable technical advices during the research project.

References

[1] Englhardt O. Leichtbau 3.0: Material, Struktur, Energie. Stahlbau; 2013. p. 421–7. https://doi.org/10.1002/stab.201310056.
[2] Martens K, Caspeele R, Belis J. Development of composite glass beams – A review. Eng Struct 2015;101:1–15. https://doi.org/10.1016/j.engstruct.2015.07.006.
[3] Luible A. Stabilität von Tragelementen aus Glas. PhD Thesis, Ecole Polytechnique Federale de Lausanne - EPFL, Switzerland; 2004.
[4] Englhardt O. Flächentragwerke aus Glas – Tragverhalten und Stabilität. PhD Thesis, University of Natural Resources and Life Sciences Vienna – BOKU, Austria; 2007.
[5] Haese A. Beitrag zur Bemessung scheibenbeanspruchter Stahl-Glas-Elemente. PhD Thesis, Universität der Bundeswehr München, Germany; 2013.
[6] Wellershoff F. Nutzung der Verglasung zur Aussteifung von Gebäudehüllen. PhD Thesis, RWTH Aachen, Germany. Aachen: Shaker; 2006. http://www.shaker.eu/shop/978-3-8322-5046-1.
[7] Freitag C, Wörner JD. Verwendung von Glas zur Aussteifung von Gebäuden. Stahlbau 2011;80:45–51. https://doi.org/10.1002/stab.201120006.
[8] Huveners E. Circumferentially adhesive bonded glass panes for bracing steel frames in facades. PhD Thesis. The Netherlands: Eindhoven University of Technology; 2009.
[9] Van Lancker B, De Corte W, Belis J. Racking stiffness and strength of cold-formed steel frames braced with adhesively bonded steel panels. Engineered Transparency 2018, Düsseldorf, Germany; 2018. p. 427–34.
[10] Van Lancker B, De Corte W, Belis J. Mechanical properties of continuous adhesive glass-steel connections under monotonic and cyclic loading. Glass Struct Eng 2018;3:197–211https://link.springer.com/article/10.1007/s40940-018-0072-y.
[11] Mocibob D. Glass panel under shear loading – use of glass envelopes in building stabilization. PhD Thesis. Switzerland: Ecole Polytechnique Federale de Lausanne - EPFL; 2009.
[12] Amadio C, Bedon C. Effect of circumferential sealant joints and metal supporting frames on the buckling behavior of glass panels subjected to in-plane shear loads. Glass Struct Eng 2016;1:353–73. https://doi.org/10.1007/s40940-015-0001-2.
[13] Steel Nhamoinesu S. Glass composite panels. PhD Thesis. United Kingdom: University of Cambridge; 2015.
[14] Pascual C, Nhamoinesu S, Overend M. The flexural response of large scale steel-framed composite glazing panels. Glass Struct Eng 2019. https://doi.org/10.1007/s40940-019-00096-4.
[15] Pascual C, Montali J, Overend M. Adhesively-bonded GFRP-glass sandwich components for structurally efficient glazing applications. Compos Struct 2017;160:560–73. https://doi.org/10.1016/j.compstruct.2016.10.059.
[16] Bedon C, Pascual C, Luna-Navarro A, Overend M, Favoino F. Thermo-mechanical investigation of novel GFRP-glass sandwich facade components. Challenging Glass 6, Delft, The Netherlands; 2018. p. 513–23.
[17] Hoffmeister B, Di Biase P, Richter C, Feldmann M. Innovative steel-glass components for high-performance building skins: testing of full-scale prototypes. Glass Struct Eng 2017;2:57–78https://link.springer.com/article/10.1007/s40940-016-0034-1.
[18] Dow Corning® 993. Structural glazing sealant – two part silicone rubber. Product data sheet, Dow Corning Corporation; 2013.
[19] SikaFast®-5221 NT. Schnelles 2-K-Klebstoffsystem für strukturelle Verklebungen. Product data sheet, Sika Österreich GmbH; 2013.
[20] Belis J, Van Hulle A, Out B, Bos F, Callewaert D, Poulis H. Broad screening of adhesives for glass-metal bonds. Glass Perform Days 2011, Tampere, Finland; 2011. p. 286–9.
[21] Overend M, Jin Q, Watson J. The selection and performance of adhesives for a steel-glass connection. Int J Adhes Adhes 2011;31:587–97. https://doi.org/10.1016/j.ijadhadh.2011.06.001.
[22] Abeln B, Preckwinkel E, Yandzio E, Heywood M, Eliasova M, Netusil M, et al. Development of innovative steel-glass structures in respect to structural and architectural design (Innoglast). Technical report. Publication office of the European Union, Luxembourg; 2013. https://doi.org/10.2777/91697.
[23] Hagl A. Die Innovation – Kleben – Aktuelles aus der "Arbeitsgruppe Kleben" des Fachverbandes Konstruktiver Glasbau – FKG. Stahlbau 2006;75:508–20. https://doi.org/10.1002/stab.200610054.
[24] Dias V, Odenbreit C, Hechler O, Scholzen F, Ben Zineb T. Development of a constitutive hyperelastic material law for numerical simulations of adhesive steel-glass connections using structural silicone. Int J Adhes Adhes 2014;48:194–209. https://doi.org/10.1016/j.ijadhadh.2013.09.043.
[25] Staudt Y, Odenbreit C, Schneider J. Failure behaviour of silicone adhesive in bonded connections with simple geometry. Int J Adhes Adhes 2018;82:126–38. https://doi.org/10.1016/j.ijadhadh.2017.12.015.
[26] Rosendahl PL, Staudt Y, Odenbreit C, Schneider J, Becker W. Measuring mode I fracture properties of thick-layered structural silicone sealants. Int J Adhes Adhes 2019;91:64–71. https://doi.org/10.1016/j.ijadhadh.2019.02.012.
[27] Rosendahl PL, Drass M, Felger J, Schneider J, Becker W. Equivalent strain failure criterion for multiaxially loaded incompressible hyperelastic elastomers. Int J Solids Struct 2019. https://doi.org/10.1016/j.ijsolstr.2019.01.030.
[28] Silvestru VA. Composite structural glazing systems – Towards transparent building envelopes with composite structural behaviour between glass panes and metal framing by adhesive bonding [PhD Thesis]. Austria: Graz University of Technology; 2018.
[29] Silvestru VA, Englhardt O, Schneider J. Investigations on linear silicone joints for glass-metal elements with composite structural behavior. Challenging Glass 2018;6:389–98.
[30] Silvestru VA, Drass M, Englhardt O, Schneider J. Performance of a structural acrylic adhesive for linear glass-metal connections under shear and tensile loading. Int J Adhes Adhes 2018;85:322–36. https://doi.org/10.1016/j.ijadhadh.2018.07.006.
[31] Ebert J. The application of heavy loads into glass edges – A contribution to the use of solid plastics as a block material. PhD Thesis. Germany: TU Dresden; 2014.
[32] Bucak O. Gutachterliche Stellungnahme für die Verwendbarkeit von Hilti HIT-HY 70 im Glasbau. Technical report. Hochschule München, Germany; 2011.
[33] Kolany G. Glas-Stahl-Konstruktionen unter Nutzung hybrider Verbundtragwirkung mit Schwerpunkt der Lasteinleitung an der Glaskante. PhD Thesis, Graz University of Technology, Austria. In progress, expected 2019.
[34] EN 10088-4. Stainless steels – Part 4: Technical delivery conditions for sheet/plate and strip of corrosion resisting steels for construction purposes; 2009.
[35] EN 10025-2. Hot rolled products of structural steels – Part 2: Technical delivery conditions for non-alloy structural steels; 2011.
[36] Abaqus 6.13: Analysis User's Guide. Dassault Systems Simulia; 2013.
[37] ÖNORM B 3716-1. Glass in building – Structural glass construction – Part 1: Basic principles; 2016.